Green's function theory for one-way particle chains

Y. Hadad, Y. Mazor, and Ben Z. Steinberg*
School of Electrical Engineering, Tel Aviv University, Ramat-Aviv, Tel-Aviv 69978, Israel
(Received 25 October 2012; revised manuscript received 7 January 2013; published 23 January 2013)

Recently, it has been shown that a new class of particle chains that support the simultaneous interplay of two-type rotations—geometric and electromagnetic—may possess strong nonreciprocity and one-way guiding effects. Here, we use the Z transform to develop a rigorous Green's function theory for these one-way chains. A study of the chain's spectra and its analytic properties in the complex spectral (Z) plane, where each and every singularity (e.g., pole, branch cut, etc.) represents a distinct wave phenomenon, reveals all the wave constituents that may be excited. We explore the breach of symmetry of the complex Z plane singularities and their manifestations as the symmetry breaking wave mechanisms that underly the one-way guiding effects. It is shown that this breach of symmetry in particle chains is possible *only* when both rotations—geometric and electromagnetic—are *simultaneously* present. It is also shown that the continuous spectrum (e.g., branch singularity) plays a pivotal role in suppressing the radiation into the "forbidden" direction.

DOI: 10.1103/PhysRevB.87.035130 PACS number(s): 41.20.Jb, 42.70.Qs, 78.67.Bf, 42.82.Et

I. INTRODUCTION

Subdiffraction chains (SDC) are linear periodic arrays of nanoparticles. They can support guided optical modes whose spatial width is smaller than the free-space wavelength λ if the interparticle distance $d < \lambda$.[1–6]

Recently, SDCs were suggested as candidates for one-way guiding on the nanoscale.[7–9] These studies include analytical models based on the discrete dipole approximation (DDA) and full-wave simulations with material loss and finite particle size verifying the one-way property for realistic parameters. The underlying physics is based on the interplay of two types of rotations: geometric and electromagnetic. Two examples are shown in Figs. 1 and 2. The first example (see Fig. 1) consists of a plasmonic-particles chain of spiral (chiral) geometry exposed to a longitudinal static magnetic field $\boldsymbol{B}_0 = \hat{\boldsymbol{z}} B_0$. Due to B_0, the chain plasmonic modes possess Faraday rotation, i.e., the dipoles in each particle rotate in the x,y plane. When such a mode interacts with the chain chirality, its nonreciprocity is strongly enhanced and a one-way guiding is created.[7] This structure has three appealing properties: (a) nanoscale transverse size, (b) propagation in the "forbidden" direction decays exponentially by about two orders of magnitude over distances of $O(\lambda)$, and (c) B_0 is weaker than that used in other magnetization-based one-way structures. However, although chiral nanochains were already fabricated,[10] they may be difficult to implement. The second example (see Fig. 2) overcomes this difficulty since it is essentially planar. Here, the chain is exposed to transverse magnetization $\boldsymbol{B}_0 = \hat{\boldsymbol{y}} B_0$, which induces *longitudinal rotation* of the SDC modes: the dipoles in each particle rotate in the x,z plane. When a *longitudinal chirality* is introduced (by using nonspherical particles that rotate in the x,z plane) two-type rotations interplay takes place and creates one-way guiding.[8]

There are numerous previous studies of different magnetization-based schemes for achieving one-way guiding. One-way total reflection from transversely infinite periodic magneto-optical layers was demonstrated in Ref. 11. In alternative approaches, the one-way property exists at the interface between two semi-infinite photonic crystals (PhC), or between a semi-infinite PhC and a metal, where at least one of these two semi-infinite structures consists of magnetooptic or gyromagnetic materials.[12–16] In all these schemes, the one-way electromagnetic edge states are supported at the interface and are assumed to be completely separated from the surrounding free space by the semi-infinite, *supposedly impenetrable* structures on both sides. Hence no radiation modes are present. As a result, an "absolute" one-way property is achieved in the sense that backscattering from obstacles is totaly eliminated.

How does the particle chain approach compare to these schemes? A complete separation from free space is a *macroscopic concept* whose microscopic validity is somewhat limited. Separation from the surrounding free space is difficult to obtain in guiding structures of nanoscale transverse dimensions. Particularly, any linear chain of nanoparticles embedded in free space or printed on dielectric layer inherently interacts with semi-infinite or infinite free spaces that surround it. There are two *major* ramifications to this fact; in addition to the well localized plasmonic modes of the chain, other types of waves are formally present. The first and widely recognized one is the presence of "light-line modes" whose dispersion follow closely the light line $\beta = \pm\omega/c$. These modes are weakly trapped by the chain, and their spatial properties are nearly those of free-space plane waves.[4] Formally, they are part of the discrete spectrum of the chain's governing operator. The second are the *continuous spectrum* (CS) waves[17] whose existence can be formally attributed to the fact that the chain's governing operator is *noncompact*, hence it possesses a CS as well. While the existence of chains discrete spectrum (modes) is easily recognized via standard dispersion analysis, the CS wave is less transparent; in analogy, this wave is reminiscent of the lateral (head) waves in open dielectric waveguides,[18,19] again governed by noncompact operators. However, despite its less transparent nature, it should not be overlooked. The CS plays a pivotal role in the *excitation* of particle chains. Its presence is the main reason for the extremely weak excitation of the light-line modes.[17]

Here, we develop a rigorous Green's function theory for nonreciprocal particle chains of the two-type rotation principle shown in Figs. 1 and 2. The theory sheds light on the

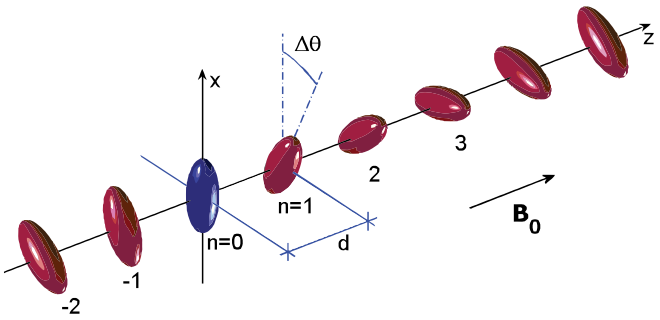

FIG. 1. (Color online) A chiral chain of plasmonic ellipsoids with longitudinal magnetization. Chirality and Faraday rotation interplay creates one-way guiding.

chain's excitation mechanisms and exposes the critical role of each wave constituent in creating the one-way guiding. Our starting point is the discrete dipole approximation (DDA).[1–6] It formally holds when the particle diameter D is much smaller than λ and when $d \gg D$. Studies show excellent agreement with exact solutions even when $d = 1.5D$.[20] Also, full wave simulations show that the DDA predicts well the one-way chains dynamics.[8,9] Then, following,[17] we use the Z- transform (ZT) to obtain a rigorous excitation theory. The result is a physically transparent tool in which the Green's function wave constituents can be discerned directly from the analytic properties of the chain's spectra in the complex Z plane. Each and every singularity (e.g., poles and branch-points/cuts) is a distinct wave phenomenon, whose excitation strength is nothing but the corresponding residue. This analytical clarity reveals the wave mechanism and content responsible for the one-way guiding. It is shown that the simultaneous presence of the two rotations is crucial for creating the symmetry breach needed for one-way guiding. Furthermore, it is shown that the CS wave—manifested by a branch point in the complex Z plane—plays a pivotal role in suppressing the radiation towards the "forbidden" direction.

The structure of the paper is as follows. A general formulation and the ZT are discussed in Sec. II. Application of the ZT to the chain in Fig. 1 is discussed in Sec. III, together with detailed analysis of the wave mechanisms leading to symmetry breach and one-way guiding. The operation of a terminated one-way chain as a nonreciprocal nanoantenna and the physical origin of novel properties that were left unexplained in Ref. 9 are also discussed. In Sec. IV, the analysis is applied to the chain shown in Fig. 2. Conclusions are provided in Sec. V.

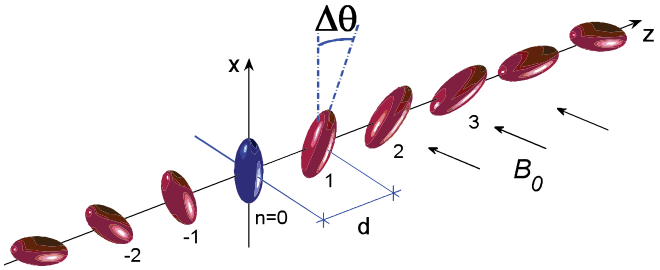

FIG. 2. (Color online) A *planar* chain of plasmonic ellipsoids with transverse magnetization and *longitudinal chirality*. It supports one-way guiding.

II. FORMULATION

Our chains are infinite linear arrays of equally spaced particles. The nth particle is located at $\boldsymbol{r}_n = (0,0,nd)$, and its electric polarizability is represented by the 3×3 matrix $\boldsymbol{\alpha}_n$. Hence its response to an exciting local field $\boldsymbol{E}^L(\boldsymbol{r}_n)$—the field at the location of the nth particle but in the absence of this particle—is faithfully described by the dipole moment $\boldsymbol{p}_n = \boldsymbol{\alpha}_n \boldsymbol{E}^L(\boldsymbol{r}_n)$. The polarizability of the reference ellipsoidal particle whose principal axes are aligned with x,y,z—the blue ellipsoid at the origin in Figs. 1 and 2—can be obtained via[21]

$$\epsilon_0 \boldsymbol{\alpha}^{-1} = V^{-1}(\boldsymbol{\chi}^{-1} + \mathbf{L}) - \frac{ik^3}{6\pi}\mathbf{I}. \tag{1}$$

Here, k is the vacuum wave number, $\mathbf{I}$ is the 3×3 identity matrix, and the imaginary term $ik^3(6\pi)^{-1}\mathbf{I}$ represents radiation loss. $V = 4\pi a_x a_y a_z/3$ is the ellipsoid volume with a_x,a_y,a_z its principal semi-axes, and $\mathbf{L} = \mathrm{diag}(N_x,N_y,N_z)$ is the depolarization matrix whose entries are obtained from a_x,a_y,a_z by elliptic integrals and satisfy $\sum_u N_u = 1$.[21] $\boldsymbol{\chi}$ is the matrix susceptibility of the ellipsoid material assumed here to be a Drude-model metal. The effect of the static magnetic field $\boldsymbol{B}_0 = B_0(\hat{\boldsymbol{x}} \sin\gamma + \hat{\boldsymbol{z}} \cos\gamma)$ is expressed in $\boldsymbol{\chi}$ by using a magnetized plasma model,[7,8,14,22]

$$\boldsymbol{\chi} = \frac{-\bar{\omega}^{-2}}{(\bar{\omega} + i\sigma)^2 - \bar{\omega}_b^2}\,\bar{\boldsymbol{\chi}}, \tag{2}$$

where $\bar{\omega} = \omega/\omega_p$, $\bar{\omega}_b = \omega_b/\omega_p$. ω_p and $\omega_b = -q_e B_0/m_e$ are the plasma and cyclotron frequencies, respectively. $\sigma = (\tau\omega_p)^{-1}$ represents loss, where τ is the dissipation time constant. $\bar{\boldsymbol{\chi}}$ is given in Appendix A. $\boldsymbol{\alpha}_n$ is obtained from $\boldsymbol{\alpha}$ by using the appropriate rotation operators. This will be discussed in the corresponding sections.

In our chains, $\boldsymbol{E}^L(\boldsymbol{r}_n)$ can be expressed as a summation over contributions from all the particles in the chain (except for the nth) plus the incident field. Therefore the entire chain response, expressed as a sequence of the particles dipole responses, is governed by the difference equation

$$\boldsymbol{\alpha}_m^{-1}\boldsymbol{p}_m - \epsilon_0^{-1}\sum_{n\neq m}\mathbf{A}[(m-n)d]\boldsymbol{p}_n = \boldsymbol{E}^i(\boldsymbol{r}_m), \tag{3}$$

where $\mathbf{A}(z)$ is the free-space dyadic Green's function, giving the electric field at $\boldsymbol{r} = (0,0,z)$ due to an infinitesimal dipole $\boldsymbol{p}$ at $\boldsymbol{r}' = \mathbf{0}$:

$$\boldsymbol{E}(z) = \epsilon_0^{-1}\mathbf{A}(z)\,\boldsymbol{p}, \tag{4}$$

$$\mathbf{A}(z) = \frac{e^{ik|z|}}{4\pi|z|}\left[k^2\mathbf{A}_1 + \left(\frac{1}{z^2} - \frac{ik}{|z|}\right)\mathbf{A}_2\right] \tag{5}$$

with $\mathbf{A}_1 = \mathrm{diag}(1,1,0)$ and $\mathbf{A}_2 = \mathrm{diag}(-1,-1,2)$. The type of chain is determined by $\boldsymbol{\alpha}_m$. In subsequent sections, Eq. (3) is transferred to a discrete convolution of the form

$$\sum_{n=-\infty}^{\infty}\mathbf{D}_{m-n}\boldsymbol{q}_n = \boldsymbol{F}_m, \tag{6}$$

where $\mathbf{D}_n$ is a sequence of matrices determined by the propagator $\mathbf{A}$ and the particle polarizabilities and where the vector sequence $\boldsymbol{q}_n$ and $\boldsymbol{F}_n$ are linearly related to the chain response $\boldsymbol{p}_n$ and to the incident field $\boldsymbol{E}^i(\boldsymbol{r}_n)$, respectively.

Due to its discrete convolution structure, the above equation can be studied and solved using the double-sided Z transform (ZT). The ZT of a *bounded* vector or matrix series is obtained by applying the conventional (scalar-series) Z transform to each of the entries. Hence

$$\hat{\boldsymbol{q}}(Z) = \sum_{n}^{\infty} \boldsymbol{q}_n \, Z^{-n} \tag{7}$$

and the transform of $\mathbf{D}_n$ is obtained similarly. The series region of convergence (ROC) is a ring that contains the unit circle $C_1: \ |Z| = 1$. The inverse ZT (IZT) is given by

$$\boldsymbol{q}_n = \frac{1}{2\pi i} \oint_{C_\pm} \hat{\boldsymbol{q}}(Z) \, Z^{n-1} dZ. \tag{8}$$

The original integration contour should reside within the ROC, and encircle the origin in a counterclockwise direction; C_1 is an appropriate path. To enhance physical insight, however, we shall replace the original contour with integrations around singularities (poles and branch cuts) of the inverse transform kernel. Thus C_1 is replaced with $C_\pm$. For observation points located at $n \geqslant 0$, the integration contour $C_\pm = C_+$ encircles all the singularities *within* C_1 in the complex Z plane in a counterclockwise direction. The contour $C_\pm = C_-$ used for $n < 0$ encircles all the singularities *external* to C_1 in the complex Z plane in a clockwise direction. The contours are shown in Fig. 3. The contributions of the different singularities may readily be used to discern between various wave species. Poles located on (off) the unit circle correspond to propagating (radiation) modes whereas branch points and cuts correspond to continuous spectrum (CS) waves.

By applying the ZT to Eq. (6), one obtains for $\hat{\boldsymbol{q}}(Z)$,

$$\hat{\boldsymbol{q}}(Z) = [\hat{\mathbf{D}}(Z)]^{-1} \, \hat{\boldsymbol{F}}(Z). \tag{9}$$

With the equation above, we define the chains Green function matrix sequence $\mathbf{G}_n$ as the IZT of $\hat{\mathbf{G}}(Z) = [\hat{\mathbf{D}}(Z)]^{-1}$,

$$\mathbf{G}_n = \frac{1}{2\pi i} \oint_{C_\pm} [\hat{\mathbf{D}}(Z)]^{-1} \, Z^{n-1} dZ. \tag{10}$$

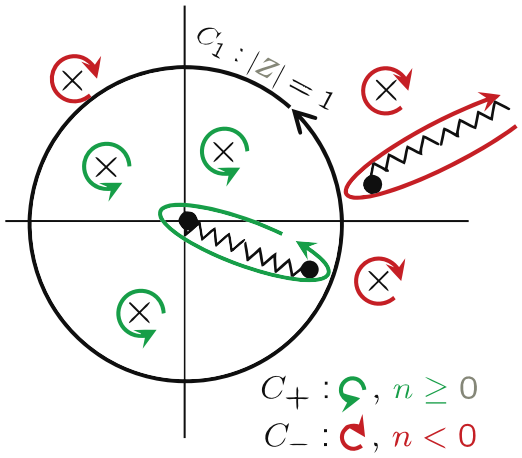

FIG. 3. (Color online) The integration contours for the IZT. Poles are marked by $\times$, branch points by $\bullet$, and branch cuts by wiggly lines. Singularities inside (outside) the unit circle contribute to $n \geqslant 0$ ($n < 0$).

This Green's function represents the chain response due to an excitation of the $n = 0$ particle by an arbitrary unit forcing vector. The chain response to an arbitrary excitation is obtained by a discrete convolution of $\mathbf{G}_n$ and the incident field forcing vector sequence $\boldsymbol{F}_m$,

$$\boldsymbol{q}_n = \sum_m \mathbf{G}_{n-m} \boldsymbol{F}_m \equiv \mathbf{G}_n * \boldsymbol{F}_n. \tag{11}$$

The chain's electrodynamics depends directly on the analytic properties of $[\hat{\mathbf{D}}(Z)]^{-1}$. Clearly,

$$[\hat{\mathbf{D}}(Z)]^{-1} = \frac{\mathrm{adj}\hat{\mathbf{D}}(Z)}{\Delta(Z)}, \tag{12}$$

where Δ and adj$\hat{\mathbf{D}}$ are the determinant and adjugate of $\hat{\mathbf{D}}$. Let Z_{p_m}, $m = 1,2,\ldots$ be the poles of the expression above. Then by applying the residue theorem we obtain from Eq. (10),

$$\mathbf{G}_n = \sum_m \mathbf{G}_n^{(p_m)} + \sum_\ell \mathbf{G}_n^{(b_\ell)}, \tag{13}$$

where $\mathbf{G}_n^{(p_m)}$ ($\mathbf{G}_n^{(b_\ell)}$) is the contribution due to the mth pole (ℓth branch point and cut). For $n \geqslant 0$ ($n < 0$), the summation is done only over singularities inside (outside) the unit circle, encircling each of these singularities in a counterclockwise (clockwise) direction, see discussion after Eq. (8) and Fig. 3. Due to the structure of the integrand in Eq. (10), the residue associated with Z_{p_m} has the general form $C(Z_{p_m}) Z_{p_m}^n$. Hence it represents the mth mode. Its excitation amplitude is $C(Z_{p_m})$ and its dispersion $\beta_m(\omega)$ is determined by

$$Z_{p_m}(\omega) = e^{i\beta_m d}. \tag{14}$$

Real β_m corresponds to a mode that propagates along the chain with no radiation to the free space and with no material loss. In this case, Z_{p_m} resides exactly on C_1 (the unit circle). Hence its classification as a singularity that contributes to $n \geqslant 0$ (encircled by C_+) or to $n < 0$ (encircled by C_-) cannot be done according to its location inside or outside C_1. Rather, this classification is done according to its *group velocity* as obtained from Eq. (14): $v_g = 1/\beta_m'(\omega) = i dZ_{p_m}/Z_{p_m}'(\omega)$. The pole contributes to $n \gtreqless 0$ and encircled by $C_\pm$ if $v_g \gtrless 0$. Alternatively, one may examine the shift in Z_{p_m} when loss is added to the system (it would shift away from the unit circle), and classify accordingly.

The branch cut contributions in Eq. (13) represent the chain's *continuous spectrum*.[17,18] They can be expressed formally as

$$\mathbf{G}_n^{(b_\ell)} = \frac{1}{2\pi i} \oint_{C_{b_\ell}} [\hat{\mathbf{D}}(Z)]^{-1} Z^{n-1} dZ, \tag{15}$$

where C_{b_ℓ} encircles the ℓth branch point and cut in the direction discussed above.

Finally, we refer to an important special case in which the entries of $\hat{\mathbf{D}}(Z)$ possess *only* branch points and cuts, with neither zeros nor poles. It holds for conventional particle chains,[17] and as we show in the next sections it applies also here. Then the poles are given only by the zeros of the determinant

$$\Delta(Z_{p_m}) = 0, \quad m = 1,2,\ldots. \tag{16}$$

By applying the residue theorem to this specific case, we get for $\mathbf{G}_n^{(p_m)}$,

$$\mathbf{G}_n^{(p_m)} = \mathrm{sign}(n)\frac{\mathrm{adj}\hat{\mathbf{D}}(Z_{p_m})}{\Delta'(Z_{p_m})} Z_{p_m}^{n-1}, \tag{17}$$

where a prime denotes derivative with respect to the argument. It can be expressed explicitly in terms of the matrix

$$\Delta'(Z) = \mathrm{Tr}\left[(\mathrm{adj}\hat{\mathbf{D}})\frac{d}{dZ}\hat{\mathbf{D}}\right]. \tag{18}$$

Finally, we note that poles may reside in the principal Riemann sheet $\mathcal{R}_0$ or in any other Riemann sheet $\mathcal{R}_m$. Pole locations depend on ω hence when ω is varied, a pole may move from $\mathcal{R}_m$ to $\mathcal{R}_{m\pm1}$ as it travels across a branch cut. Formally, only poles in $\mathcal{R}_0$ contribute to the sum in Eq. (13). However, in some applications, one may find advantages in deforming the original integration contour into other Riemann sheets or in deforming the branch cut, especially if a steepest descent path (SDP) can be found in oscillatory integrands.[19] In such cases, the deformed path may sweep across a pole singularity out of $\mathcal{R}_0$ (i.e., the singularity is caught between the original and the deformed paths), leading to a spurious (implicit) inclusion of its residue. Then one needs to compensate for the spurious inclusion, leading to the so-called "improper pole" contribution that is limited to confined regions in space and can be given ray or mode interpretations (depending on the SDP deformation). Improper modes in the context of particle chains were studied in Ref. 23. It should be emphasized, however, that in our formulation, there is no SDP, and improper pole contribution does not exist. In the next sections, we use the tools above to explore the wave constituents associated with our one-way chains.

III. LONGITUDINAL MAGNETIZATION, CONVENTIONAL CHIRALITY

Here, we study the chain described by Fig. 1. $\boldsymbol{\alpha}$ and $\boldsymbol{\chi}$ are given by Eqs. (1) and (2) and Eq. (A 1) with $\gamma = 0$. The polarizability of the nth particle is $\boldsymbol{\alpha}_n = \mathbf{T}_{-n}\boldsymbol{\alpha}\mathbf{T}_n$. Here, $\mathbf{T}_n$ is a transverse rotation operator (rotates by $n\Delta\theta$ about $\hat{\boldsymbol{z}}$) whose nonzero entries are $t_{11} = t_{22} = \cos n\Delta\theta, t_{33} = 1, t_{12} = -t_{21} = \sin n\Delta\theta$. We substitute this expression for $\boldsymbol{\alpha}_m$ into Eq. (3), apply $\mathbf{T}_m$ on both sides, use the identities $\mathbf{T}_m^{-1} = \mathbf{T}_{-m}$, $\mathbf{T}_m = \mathbf{T}_{m-n}\mathbf{T}_n$, and the fact that $\mathbf{T}_n$ *commutes with* $\mathbf{A}$ (here, the field on the chain axis due to a rotated dipole is the rotated field of the reference dipole). The result is the convolution (6) where

$$\boldsymbol{q}_n = \mathbf{T}_n\boldsymbol{p}_n, \quad \boldsymbol{F}_m = \mathbf{T}_m\boldsymbol{E}^i(\boldsymbol{r}_m), \tag{19}$$

and

$$\mathbf{D}_n = \begin{cases} -\epsilon_0^{-1}\mathbf{A}(nd)\mathbf{T}_n, & n \neq 0, \\ \boldsymbol{\alpha}^{-1}, & n = 0. \end{cases} \tag{20}$$

This is a description in a reference frame that rotates together with the chain. $\mathbf{T}_n$ leaves the $\hat{\boldsymbol{z}}$ polarization unchanged. Also, as $\gamma = 0$, Eqs. (A1e) and (A1f) vanish, leaving only $\bar{\chi}_{zz}$ in the third row and column of $\bar{\boldsymbol{\chi}}$. Hence, the $\hat{\boldsymbol{z}}$ polarization in our chain is very similar to that of a chain with nonmagnetized plasmonic spheres; the only change is a shift in the resonance frequency due to the presence of $\bar{\omega}_b$ and due to the depolarization factor N_z, which is different than that of a sphere (1/3). This is clear, as $\boldsymbol{B}_0 = B_0\hat{\boldsymbol{z}}$ couples only the $\hat{\boldsymbol{x}}, \hat{\boldsymbol{y}}$ polarizations. Therefore, for simplicity, we concentrate only on the transverse polarizations and ignore the third row and column of the chain equation, and deal only with the upper 2×2 blocks in the matrix-series equation above. We have for the ZT of $\mathbf{D}_n$ (use $\mathbf{T}_{\pm n} = \mathbf{T}_1^{\pm n}$),

$$\hat{\mathbf{D}}(Z) = \boldsymbol{\alpha}^{-1} - \epsilon_0^{-1}\sum_{n=1}^{\infty}\mathbf{A}(nd)[(\mathbf{T}_1 Z)^{-n} + (\mathbf{T}_1 Z^{-1})^{-n}]. \tag{21}$$

After some algebra, this gives

$$\hat{\mathbf{D}} = \boldsymbol{\alpha}^{-1} - \mathbf{C}, \quad \mathbf{C} = \begin{bmatrix} C_c & C_x \\ -C_x & C_c \end{bmatrix} \tag{22}$$

with

$$C_{c,x}(Z) = \frac{k^3}{8\pi\epsilon_0}\sum_{n=1}^{3}\frac{a_n^{c,x}}{(kd)^n} f_n^{c,x}(Z), \tag{23}$$

where $a_n^c = i^{n-1}$, $a_n^x = -ia_n^c$ and

$$f_s^c(Z) = Li_s[e^{i(kd+\Delta\theta)}Z^{-1}] + Li_s[e^{i(kd-\Delta\theta)}Z^{-1}] + Li_s[e^{i(kd+\Delta\theta)}Z] + Li_s[e^{i(kd-\Delta\theta)}Z], \tag{24a}$$

$$f_s^x(Z) = Li_s[e^{i(kd+\Delta\theta)}Z^{-1}] - Li_s[e^{i(kd-\Delta\theta)}Z^{-1}] - Li_s[e^{i(kd+\Delta\theta)}Z] + Li_s[e^{i(kd-\Delta\theta)}Z]. \tag{24b}$$

$Li_s(z)$ is the sth order polylogarithm function[24]

$$Li_s(z) = \sum_{n=1}^{\infty}\frac{z^n}{n^s} \Rightarrow Li_s'(z) = z^{-1}Li_{s-1}(z), \tag{25}$$

with $Li_0(z) = z/(1-z), Li_1(z) = -\ln(1-z)$. While the sum in Eq. (25) converges formally only for $|z| < 1$, it can be extended into the entire complex plane via analytic continuation. $Li_s(z)$ has neither poles nor zeros, only branch-point singularities.[24] This implies that the elements of $\hat{\mathbf{D}}(Z)$ have no poles nor zeros, as stated in the discussion preceding Eq. (16). Additional properties of the polylogarithm functions needed here are presented in Refs. 8 and 17. Generally, $Li_s(z)$ inherits the singularity of $\ln(1-z)$ $\forall s \geqslant 1$, possessing Riemann sheets of infinite multiplicity $\mathcal{R}_m, m = 0, \pm1, \pm2\ldots$ with branch points at $z = 1$. Hence, in the zeroth (or principle) Riemann sheet, $\mathcal{R}_0$ $f_s^c(Z)$ and $f_s^x(Z)$ possess four branch points $Z_{b\,1,2,3,4}$ and corresponding branch cuts,

$$Z_{b\,1,3} = e^{\mp i(kd+\Delta\theta)}, \quad Z_{b\,2,4} = e^{\mp i(kd-\Delta\theta)}. \tag{26}$$

Consistently with the logarithmic functions, two cuts emerge from the branch points at $Z_{b\,1,2}$ and extend to the origin, and other two cuts emerge from the branch points at $Z_{b\,3,4}$ and extend to infinity. These branch points result solely from the analytic properties of the Polylogarithm functions (which in turn result from interparticle interactions). Hence they are *independent of the particle material*. This fact is of importance for understanding the complete chain behavior in the presence of loss. The Green's function analytic properties and the various wave constituents supported by the chain are completely determined by the expressions above.

A. Analytic properties, symmetries, and wave constituents

The Green's function spectrum $\hat{\mathbf{G}}(Z) = [\hat{\mathbf{D}}(Z)]^{-1}$ is given generally in Eq. (12). Here,

$$\Delta(Z) = \hat{D}_{xx}\hat{D}_{yy} - \hat{D}_{xy}\hat{D}_{yx}, \tag{27a}$$

$$\mathrm{adj}\hat{\mathbf{D}}(Z) = \begin{pmatrix} \hat{D}_{yy} & -\hat{D}_{xy} \\ -\hat{D}_{yx} & \hat{D}_{xx} \end{pmatrix}. \tag{27b}$$

The adj$\hat{\mathbf{D}}$ entries have neither poles nor zeros, hence Eqs. (16)–(18) apply. The entries possess only branch-point singularities, which are given in Eq. (26). The determinant Δ inherits these very same points. In addition, it has eight zeros which are poles of $[\hat{\mathbf{D}}(Z)]^{-1}$, given by Eq. (16) with $m = 1,\ldots,8$. They represent the chain *discrete spectrum*—the chain modes—see Eq. (14). The excitation magnitude of these modes is nothing but the associated residue given generally in Eq. (17). Finally, the branch points in Eq. (26) and the associated branch cuts represent the chain's *continuous spectrum* (CS).[17,18]

By using the property in Eq. (25), $\Delta'(Z)$ can be expressed explicitly in terms of Li_s in a structure similar to Eqs. (23) and (24). This is presented in Sec. A 2 in Appendix A. We note that the branch points and cuts of $\Delta'(Z)$ are identical to those of $f_n^{c,x}(Z)$, and are given in Eq. (26) and the discussion thereafter. Furthermore, from Sec. A 2, we have

$$\lim_{Z/Z_b = x \to 1} \frac{1}{\Delta'(Z)} = C\frac{(1-x)}{\ln(1-x)} \to 0 \tag{28}$$

that is essential for understanding the CS role in suppressing the modal propagation towards the "forbidden" direction in one-way chains.

From the discussions and results above, it follows that analytic investigation of the matrix function $\hat{\mathbf{D}}^{-1}$ is reduced to an investigation of the scalar function $\Delta(Z)$ and its singularities. From Eqs. (16)–(18), (23), (24), and (A2)–(A4), we reach the following observations.

(1) $\hat{D}_{uu}(Z) = \hat{D}_{uu}(Z^{-1})$, where $u = x$ or y.

(2) For $\Delta\theta \neq 0$, $f_s^x(Z) = -f_s^x(Z^{-1}) \Rightarrow C_x(Z) = -C_x(Z^{-1})$.

(3) Without rotation, $\Delta\theta = 0$, $f_s^x(Z) \equiv 0 \Rightarrow \hat{D}_{xy} = -\hat{D}_{yx} = [\boldsymbol{\alpha}^{-1}]_{xy}$ Z independent.

(4) Without magnetization $[\boldsymbol{\alpha}^{-1}]_{uv|_{u\neq v}} = 0$. Hence, from Eq. (22), $\hat{D}_{uv}(Z) = -\hat{D}_{vu}(Z)$. Also, by observation 2, $\hat{D}_{uv}(Z) = -\hat{D}_{uv}(Z^{-1})$ hence $\hat{D}_{uv}\hat{D}_{vu}(Z) = \hat{D}_{uv}\hat{D}_{vu}(Z^{-1})$ where $u \neq v$, $u,v = x$ or y.

(5) With magnetization $[\boldsymbol{\alpha}^{-1}]_{uv|_{u\neq v}} \neq 0 \Rightarrow \hat{D}_{uv}\hat{D}_{vu}(Z) \neq \hat{D}_{uv}\hat{D}_{vu}(Z^{-1})$, where $u,v = x$ or y.

(6) From Eq. (26), the branch points come in pairs independently of magnetization or rotation: $Z_{bn} = 1/Z_{bn+2}$, $n = 1,2$. Without rotation, Z_{bn} coincides with Z_{bn+1}.

(7) From Eqs. (17), (28), and the fact that $\hat{\mathbf{D}}(Z_{p_m})$ has only logarithmic singularity, $\lim_{Z_{p_m}\to Z_b} \mathbf{G}_n^{(p_m)} = 0$. That is, if a pole approaches a branch point, its residue is vanishingly small (see below for numerical values).

Consider first a chain of nonrotating ellipsoids (whether magnetized or not). By observations 1 and 3 above, we conclude that $\Delta(Z) = \Delta(Z^{-1})$. Namely, singular points come in pairs and therefore to each forward propagating wave there is a backward propagating counterpart, both having the same dispersion (inverse poles) and the same absolute magnitude (same residues). The specific vector structures of the modes are determined by adj$\hat{\mathbf{D}}$. With no magnetization the vectors corresponding to $\pm\hat{z}$ propagation are exactly the same. In case that the chain is magnetized, these vectors possess $\pm\pi/2$ phase difference between p_x and p_y, thus the waves experience Faraday rotation and the chain can be considered as weakly nonreciprocal. Next, consider a nonmagnetized spiral chain. By observation 4, we conclude that the symmetry $\Delta(Z) = \Delta(Z^{-1})$ still holds and the structure is reciprocal. The singularities map of this case is shown in Fig. 4. For simplicity, we assume now that $\sigma = 0$ (no loss). Referring to the figure, branch points are shown by solid black circles, branch cuts by wiggly lines, and poles are marked by black $\times$, all for a specific frequency. Poles trajectories as a function of frequency are denoted by solid color lines in the zeroth Riemann sheet $\mathcal{R}_0$. Pole locations at critical frequencies are marked by numbers. Outside $\mathcal{R}_0$ poles have no significant importance since they do not contribute. Therefore trajectory sections in these sheets were omitted for the sake of clarity (only one exception for demonstration, shown by dashed line in the figure). In addition, the evolution of the branch points as a function of frequency as given in Eq. (26) is omitted to avoid cluttering the figure. Following Eq. (14) and the discussion thereafter, the dispersion curves for poles that reside on C_1 are shown in the inset of Fig. 4, color coded according to the corresponding pole trajectories. The critical frequency marked by ω_i corresponds to the ith critical point in the pole trajectory. Note that the critical frequencies $\omega_2,\ldots,\omega_5$ represent

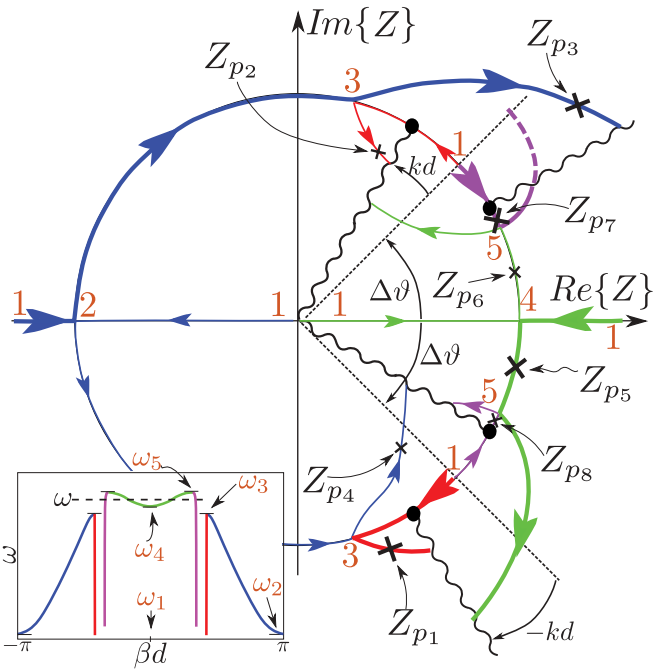

FIG. 4. (Color online) Maps of singularities in $\mathcal{R}_0$ for spiral nonmagnetized chain. There are eight poles, four of them denoted by thin (thick) lines correspond to modes with positive (negative) group velocity. Note the symmetric locations of the poles that indicate the reciprocal nature of the system. The dispersion for poles that reside on C_1 are shown in the inset, color coded according to the pole trajectories. ω_i corresponds to the ith critical point in the pole trajectory.

points where two first-order pole trajectories coincide (thus creating a higher-order pole) and then *bifurcate* to first-order poles again.

As pointed before, there are eight poles. We denote by $Z_{p\,1,3,5,7}$ ($Z_{p\,2,4,6,8}$) the poles pertaining to propagation in $n<0$ ($n\geqslant 0$). At very low frequencies, four poles $Z_{p\,1,2,7,8}, Z_{p\,1,7}=Z_{p\,2,8}^{-1}$ are located in $\mathcal{R}_0$ on C_1 near $Z=e^{i(\pm\Delta\theta\pm kd)}$ at location 1. Their location indicates they correspond to propagation modes of the chain, with characteristic dispersion very close to the light line ("light-line poles"). They possess no low-frequency cutoff, and their evolution with frequency is shown by the red and purple lines. For $\omega<\omega_3$, their location remains close to the brunch points [the latter evolve along C_1, see Eq. (26)]. Note that by observation 7, the corresponding residues are very small, see below. These poles correspond to "light-line modes" that poorly interact with the chain and exist as a background plane waves.

Four additional poles, $Z_{p\,3,4}$ with $Z_{p\,3}=Z_{p\,4}^{-1}$ ($Z_{p\,5,6}$ with $Z_{p\,5}=Z_{p\,6}^{-1}$) emerge from $Z=-\infty$ and from the origin (from $Z=\infty$ and the origin) in $\mathcal{R}_0$ and move along the blue (green) trajectories towards $Z=-1$ ($Z=1$). They reach point 2 (4) where Z_{p3} and Z_{p4} (Z_{p5} and Z_{p6}) meet at frequency $\omega_2(\omega_4)$ and *bifurcate* to trajectories on C_1, representing the lower cutoff of the corresponding chain propagating modes. As frequency increases, all these eight poles evolve along C_1 towards points 3 (5). The corresponding frequency $\omega_3(\omega_5)$ is the upper cutoff of the chain modes. For $\omega>\omega_3$ ($\omega>\omega_5$), the poles represent radiation modes that move along the red and blue (purple and green) trajectories, intersect the branch cuts and stop contributing. It should be emphasized that for sufficiently large frequencies, there exist no poles in $\mathcal{R}_0$ and the chain Green's function consists of branch cut (i.e., CS) contribution only; in this frequency domain, no propagation modes or radiation modes are supported by the chain. Finally, note that when losses are present $Z_{p\,1,3,5,7}$ ($Z_{p\,2,4,6,8}$) are slightly shifted outwards (inward) of C_1, but the branch point locations are not affected.

Once the spiral structure is magnetized, the symmetry disappears. This pivotal difference can be inferred from observations 1 and 5, and can clearly be seen in Fig. 5. We have $\Delta(Z)\neq\Delta(Z^{-1})$, in this case, pole singularities *do not come in pairs*. Thus the (complex) phase coefficients of the forward and backward propagating modes are different and consequently the structure's electrodynamics is strongly nonreciprocal. The dispersion curves derived from Eq. (14) for the poles that reside on C_1 are shown in the figure's inset. Regarding the CS; the branch points, which are material independent, are still located symmetrically according to Eq. (26). However, this fact alone does not result in reciprocal CS waves since the Green's function spectrum along the cuts is not symmetric as before.

To demonstrate enhanced nonreciprocity and one-way guiding, let us examine the picture at the frequency ω_l, for which the poles are marked (by $\times$) in the figure. As mentioned already, there are eight poles. Four of these, $Z_{p\,2,4,6,8}$ (denoted by thin lines), correspond to modes with positive group velocity (propagation toward $+z$). Three of them, $Z_{p\,2,4,6}$, reside off C_1 hence they are radiation modes that decay exponentially along the chain. The fourth, Z_{p8}, is poorly excited as it

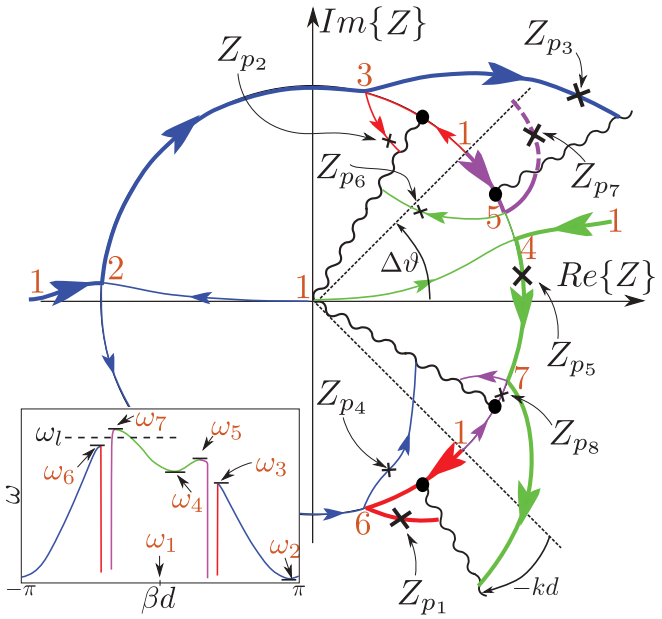

FIG. 5. (Color online) Maps of singularities for spiral and magnetized chain. There are eight poles, four of them denoted by thin (thick) lines correspond to modes with positive (negative) group velocity. Note the nonsymmetric locations of the poles which indicate the strong nonreciprocal nature of the system. The dispersion of poles that reside on C_1 are shown in the inset together with the critical frequencies.

resides very close to a branch point (recall previous discussion and observation 7). Other four poles, $Z_{p\,1,3,5,7}$ (denoted by thick lines), correspond to modes with negative group velocity (propagation toward $-z$). Two of them, $Z_{p\,1,3}$, reside off C_1 hence they correspond to exponentially decaying radiation modes. The third, $Z_{p\,7}$, is located in different Riemman sheet and therefore does not contribute at all. Thus, finally, we observe a significant, propagating mode contribution, only from the fourth pole, Z_{p5}, contributing only to $n<0$. In Fig. 6, we show the residues of Z_{p8} and Z_{p5}, the two poles that reside on C_1. The chain parameters are $d=\lambda_p/30$, where λ_p is the wavelength associated with the plasma frequency ω_p. The ellipsoids semiaxes are $a_x=0.25d$, $a_y=a_z=0.5a_x$. Chain rotation step $\Delta\theta=70^\circ$, and magnetization is $\omega_b=0.01\omega_p$. The dominance of $\mathrm{Res}Z_{p5}$ over $\mathrm{Res}Z_{p8}$ due to the proximity of the latter to the CS, is in evident. The residue of Z_{p8} is exponentially weaker (note the logarithmic scale), and at the critical frequency ω_6 that represents the lower end of the one-way band (see inset in Fig. 5) it is nearly six orders of magnitude smaller. Hence the strong nonreciprocity and preference of the $n<0$ range. These conclusions are demonstrated numerically below. Figure 7 shows the Green's function Dyad and its components for $\hat{\mathbf{y}}$-polarized excitation. The chain parameters are the same as those used for Fig. 6 (detailed above), and the frequency is shown by the vertical dash-dot line in Fig. 6. Figure 7(a) shows the total response. The propagation into the $n>0$ domain decays exponentially to a relative level of 10^{-3} within a range of less then 4λ. Figure 7(b) shows the contribution of the CS. In the domain near the source (e.g., $|z|<\lambda$) the CS wave is significant, but it decays away from the source. Note that for $n\geqslant 0$ ($n<0$)

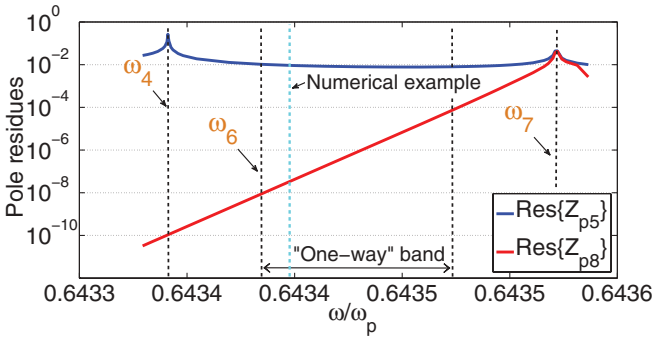

FIG. 6. (Color online) Residues of Z_{p5} and Z_{p8}, representing modes excitation magnitudes. The locations of critical frequencies from the inset of Fig. 5 are shown. Within a finite frequency band, the excitation magnitude of the mode that propagates in the "forbidden" direction is orders of magnitude weaker than that of the mode that propagates in the "allowed" direction. This is due to the proximity of the former to the CS wave (branch point). The one-way domain is defined as the region where the residues ratio is below 10^{-2}. The numerical example below is at the frequency shown by the vertical dash-dot line.

only the cuts inside (outside) the unit circle contribute, but although the associated branch points always reside on the unit circle the former cuts contribution is considerably weaker than that of the latter. The reason is that the integrand itself lost its symmetry in the complex Z plane. Finally, Fig. 7(c) shows the pole contributions. For $n < 0$, there is a significant contribution due to the pole Z_{p5} that resides on the unit circle and corresponds to a guided mode of the chain. All other modes that contribute to $n < 0$ reside outside the unit circle hence they decay exponentially and their contribution cannot be seen in the graph. Pole contributions for $n \geqslant 0$ decay exponentially since all the relevant poles reside inside the unit circle, except for pole Z_{p8}, which is practically not excited due to its proximity to the branch point.

To summarize, symmetry in the spectral plane is broken only under the simultaneous presence of rotation and magnetization. Under this breach of symmetry, the proximity of a

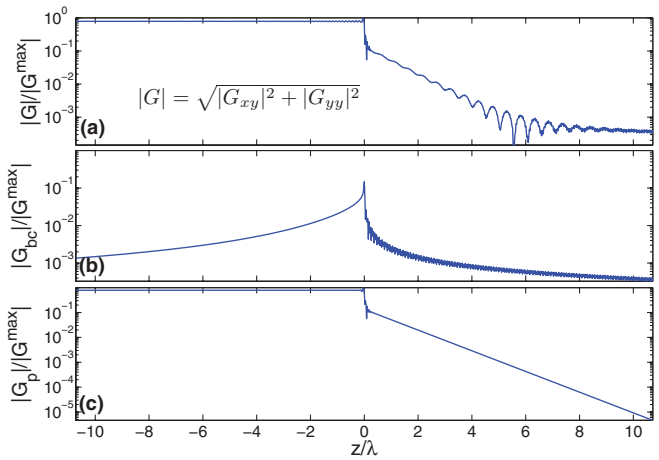

FIG. 7. (Color online) Relative magnitudes of (a) the chain Green's function and its components, (b) CS, and (c) Poles (modes).

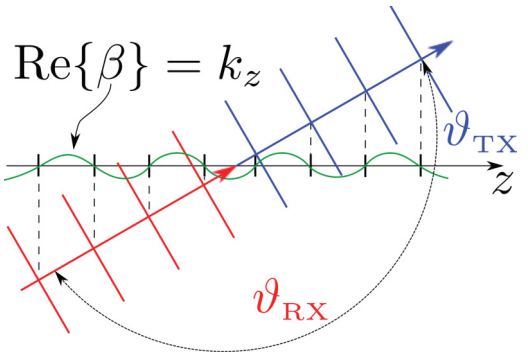

FIG. 8. (Color online) A single leaky mode with longitudinal wave number β transmits to and receives from opposite directions.

pole to the branch point (or CS) is responsible for "shutting down" the wave constituents that propagate in the "forbidden" direction.

B. A terminated one-way waveguide

Recently, full-wave simulations were used to demonstrate that a terminated one-way waveguide can be viewed as a matched nonreciprocal waveguide-antenna assembly.[9] It exhibits a novel property that was left unexplained: it transmits to and receives from *complementary* directions, i.e., $\theta_{Tx} + \theta_{Rx} = 180^\circ$. This property can be explained by the *asymmetric* spectral maps revealed in the previous section.

First, recall the basic principle of this nanoantenna. Under one-way operation, there is only one propagating mode, and only in one direction, since there is only one pole located on the unit circle in Fig. 5 that can be practically excited. As it hits a termination, back-reflections cannot take place and the mode is converted to leaky modes and CS waves—all of which are radiating waves. Hence the terminated one-way chain acts as a waveguide that over the entire one-way frequency band is perfectly matched to an antenna; the latter consists of a limited number of particles near the termination. Moreover, the guided mode conversion to CS is minor compare to its conversion to leaky modes as the guided mode longitudinal wave number is much larger than that of the CS $\beta_g \gg k$. Thus it is essentially a leaky wave antenna.

Consider now a *single* leaky mode due to the single pole Z_p, and its corresponding chain wave number β as given in Eq. (14). In order to couple to a plane wave that radiates at an angle θ_{Tx}, the phase-matching condition $\mathrm{Re}(\beta) = k\cos(\theta_{Tx})$ has to be satisfied. Therefore, if a leaky mode transmits toward θ_{Tx}, then its excitation due to an impinging plane wave is maximized if the latter hits from $\theta_{Rx} = 180^\circ - \theta_{Tx}$. See Fig. 8 for demonstration. In conventional, reciprocal, leaky wave antennas—leaky modes come in pairs with opposite longitudinal wave numbers β and $-\beta$. Assuming that the β mode transmits at (receives from) θ_{Tx} (θ_{Rx}) then the $-\beta$ mode receives from (transmits at) that angle. Therefore the radiation patterns in transmit and receive are eventually identical. However, as we consider one-way waveguides, this nice $\beta, -\beta$ symmetry breaks yielding that the radiation patterns in Tx and Rx remain as of a single leaky mode, i.e., in complementary directions as in Ref. 9.

IV. TRANSVERSE MAGNETIZATION, LONGITUDINAL CHIRALITY

We turn to the chain shown in Fig. 2. $\boldsymbol{\alpha}$ and $\boldsymbol{\chi}$ are given by Eqs. (1) and (2) and Eq. (A 1) with $\gamma = -\pi/2$. The polarizability of the nth particle is $\boldsymbol{\alpha}_n = \mathbf{T}^{\ell}_{-n}\boldsymbol{\alpha}\mathbf{T}^{\ell}_{n}$. Here $\mathbf{T}^{\ell}_{n}$ is a *longitudinal* rotation operator (rotates by $n\Delta\theta$ about $\hat{\boldsymbol{y}}$) with the nonzero entries $t_{11} = t_{33} = \cos n\Delta\theta$, $t_{22} = 1$, $t_{13} = -t_{31} = \sin n\Delta\theta$. Note, however, that unlike the chain of Fig. 1, here $\mathbf{T}^{\ell}_{n}$ and $\mathbf{A}$ of Eqs. (4) and (5) *do not commute*. Hence, while the previous chain can be regarded as periodic with period d (in the rotating reference frame) for *any* $\Delta\theta$, the present chain is periodic only for rational $\Delta\theta/\pi$. For this reason, the route from the general chain formulation in Eq. (3) to the shift-invariant formulation in Eq. (6) is more elaborated. Towards this end, we limit our discussion to cases where $\Delta\theta/\pi$ is rational. Then the chain is $D = Nd$-periodic, consists of N particles with polarizabilities $\boldsymbol{\alpha}_0, \boldsymbol{\alpha}_1, \ldots, \boldsymbol{\alpha}_{N-1}$ in a period. Also, note that the static magnetic field $\boldsymbol{B}_0 = B_0\hat{\boldsymbol{y}}$ couples the $\hat{\boldsymbol{x}}, \hat{\boldsymbol{z}}$ polarized dipole moments, but except for a shift in the resonance frequency it leaves the $\hat{\boldsymbol{y}}$ polarization essentially unchanged compare to the case of a conventional chain of spherical particles. Hence, we concentrate only on the $\hat{\boldsymbol{x}}, \hat{\boldsymbol{z}}$ components of the matrices and vectors involved.

To get a shift invariant formulation, we define the sequence of unknown vectors $\boldsymbol{q}_n$ as the dipole moments excited in the nth period:

$$\boldsymbol{q}_n = (\boldsymbol{p}_{Nn}, \boldsymbol{p}_{Nn+1}, \ldots, \boldsymbol{p}_{Nn+N-1}), \tag{29}$$

this vector consists of $2N$ scalar unknowns. Then, by rearranging Eq. (3), we get the formulation in Eq. (6) with the matrix sequence $\mathbf{D}_m$ that consists of $N \times N$ block matrices of 2×2 each, denoted $[\mathbf{D}_n]_{pl}$, $p,l = 1, \ldots N$,

$$[\mathbf{D}_n]_{pl} = \begin{cases} \boldsymbol{\alpha}_p^{-1}, & n = 0, \quad p = l, \\ -\epsilon_0^{-1}\mathbf{A}(nNd + [l-p]d), & \text{else.} \end{cases} \tag{30}$$

The right-hand side vector of Eq. (6), $\boldsymbol{F}_m$ is given by the incident electric field $\boldsymbol{E}^i(\boldsymbol{r}_m)$ arranged as $\boldsymbol{p}_m$ in Eq. (29). We apply now the ZT to the resulting formulation. The ZT of the sequence of matrices may be obtained by following essentially the same steps as in Sec. III, together with the analysis presented in Ref. 8 (particularly, see derivations leading from Eq. (8) to Eq. (13) in Ref. 8, and use $e^{i\beta d} \mapsto Z$). The result is a $2N \times 2N$ matrix $\hat{\mathbf{D}}(Z)$ that consists of $N \times N$ blocks of 2×2 submatrices $\hat{\mathbf{D}}_{pq}(Z)$, $p,q = 0, \ldots, N-1$ that are given by

$$\hat{\mathbf{D}}_{pq}(Z) = \begin{cases} \boldsymbol{\alpha}_p^{-1} - \epsilon_0^{-1}\mathbf{S}_0(Z), & p = q, \\ -\epsilon_0^{-1}\mathbf{S}_{p-q}(Z), & p \neq q, \end{cases} \tag{31}$$

where

$$\mathbf{S}_0(Z) = \frac{k^3}{4\pi}\sum_{n=1}^{3} u_n \frac{f_n(kNd, Z)}{(kNd)^n}\mathbf{A}_n, \tag{32}$$

and where $(u_1, u_2, u_3) = (1, -i, 1)$, the matrices $\mathbf{A}_n$ are the same as in Eqs. (4) and (5) with $\mathbf{A}_3 = \mathbf{A}_2$ and with the second row and column omitted (see discussion in the opening paragraph of Sec. IV), and f_n are given by

$$f_n(x, Z) = Li_n(e^{ix}Z) + Li_n(e^{ix}Z^{-1}). \tag{33}$$

The matrices $\mathbf{S}_q(Z)$, $q = \pm 1, \pm 2 \ldots, \pm(N-1)$ are given by the same summation as for $\mathbf{S}_0$ in Eq. (32), but with $f_n(kNd, Z)$ replaced by the functions $h_n(kd, Z, q)$

$$h_n(kd, Z, q) = \frac{Z^{q/N}}{N}\sum_{r=0}^{N-1} e^{-i2\pi rq/N} f_n(kd, Z^{1/N}e^{-i2\pi r/N}). \tag{34}$$

From Eqs. (31) and (34), it follows that all the components of $\hat{\mathbf{D}}(Z)$ are given by finite sums of Polylogarithm functions. Hence they inherit exactly the same branch point and branch cut singularities discussed in Sec. III. Apparently, there is an additional branch point and cut associated with the $Z^{1/N}$ term in Eq. (34). However, despite this branch singularity that creates Riemann sheets of N multiplicity (i.e., $Z^{1/N} \neq (Ze^{i2\pi m})^{1/N}, m = 1, \ldots N-1$), *the functions h_n are analytic across the cut*. This is evident from the following identity (see proof in Appendix B):

$$h_n(kd, Z, q) = h_n(kd, Ze^{i2\pi m}, q), \tag{35}$$

for all integer m. Hence this cut does not show up in our Green's function spectra and it can be ignored.

The results above express the Z-transformed chain matrix $\hat{\mathbf{D}}$ in terms of finite sums of polylogarithmic functions Li_s—defined in Eq. (25) and discussed thereafter. Recall $Li_s(z)$ possess neither poles nor zeros and inherit only the branch-point singularity of $\ln(1-z)$. Hence, as the branch point and cut associated with the $Z^{1/N}$ argument in Eq. (34) do not survive, we are left only with those associated with f_n in Eqs. (32) and (34). Hence, in the complex Z plane, $\hat{\mathbf{D}}(Z)$ and $[\hat{\mathbf{D}}(Z)]^{-1}$ have only two branch points

$$Z_{b\,1,2} = e^{\mp iNkd}. \tag{36}$$

Consistently with the logarithmic functions, the first (second) branch extends from $Z_{b\,1}$ ($Z_{b\,2}$) to the origin (infinity).

A. Analytic properties, symmetries, and wave constituents

As in the previous case, since the entries of $\hat{\mathbf{D}}$ possess neither poles and no zeros, poles are obtained only as the zeros of the determinant $\Delta(Z)$. Contributions from poles are expressed generally in Eq. (17). Branch cut/CS are given now in Eq. (36) and their contribution is expressed generally in Eq. (15). However, since $\hat{\mathbf{D}}(Z)$ is a $2N \times 2N$ matrix, explicit expressions of the Green's function spectra $\hat{\mathbf{D}}^{-1}(Z)$ cannot be obtained. Nevertheless, some general and important properties can be discerned directly from the structure of the matrices involved, for any N. First, note the symmetries of $f_n(x, Z)$ and $h_n(x, Z, q)$. We have

$$f_n(x, Z^{-1}) = f_n(x, Z), \tag{37a}$$

$$h_n(x, Z^{-1}, q) = h_n(x, Z, -q). \tag{37b}$$

Equation (37a) follows straightforwardly from Eq. (30), and Eq. (37b) is proved in Appendix C. The results above imply the symmetries of the matrices $\mathbf{S}_q$ [see Eqs. (32)–(34)]:

$$\mathbf{S}_q(Z^{-1}) = \mathbf{S}_{-q}(Z), \quad q = 0, \quad \pm 1, \ldots \pm(N-1). \tag{38}$$

Note that $\mathbf{S}_q$ are the block matrices of the Z-transformed matrix $\hat{\mathbf{D}}(Z)$, see Eq. (31). Furthermore, $\mathbf{S}_q$ are independent

of the magnetization. The latter affects $\boldsymbol{\alpha}$ only. The following observations can be made.

(1) For nonmagnetized particles, $\boldsymbol{\alpha}_n = \boldsymbol{\alpha}_n^T$ with or without particle rotation. Hence from Eq. (31) and Eq. (38), we have $\hat{\mathbf{D}}(Z^{-1}) = [\hat{\mathbf{D}}(Z)]^T$. This implies $\mathrm{Det}\{\hat{\mathbf{D}}(Z^{-1})\} = \mathrm{Det}\{\hat{\mathbf{D}}(Z)\}$ or $\Delta(Z) = \Delta(Z^{-1})$.

(2) For magnetized chain and without rotation, we have $N = 1$, and $\hat{\mathbf{D}}$ is a 2×2 matrix [only the first row in Eq. (31)]. The off-diagonal terms are only due to $\boldsymbol{\alpha}_0$ (Z independent), with $\hat{D}_{xz} = -\hat{D}_{zx}$. Since only $\mathbf{S}_0$ in Eq. (32) survives, we again have $\Delta(Z) = \Delta(Z^{-1})$.

(3) When magnetization *and* rotation are present, $\boldsymbol{\alpha}_n \neq \boldsymbol{\alpha}_n^T$. Hence, despite the inherent symmetry in Eq. (38), we have $\Delta(Z) \neq \Delta(Z^{-1})$.

(4) Due to Eq. (18) and the structure of the elements of $\hat{\mathbf{D}}$ in Eqs. (30)–(34), we have $\lim_{Z \to Z_b} \Delta' = \infty$ [note that $Li_1'(z) = (1-z)^{-1}$ and that adj$\hat{\mathbf{D}}$ has no poles]. Hence, as in the previous case, if a pole approaches a branch point, its residue is vanishingly small.

From observations 1–3, it is clear that if rotation *and* magnetization are *not* simultaneously present, symmetry in the complex Z plane is preserved: if $Z = Z_{p_m}$ is a pole, then so is $Z = Z_{p_m}^{-1}$, with the same residue. The same applies for the CS wave. *Symmetry is broken only when rotation and magnetization are simultaneously present.* Under this breach of symmetry, observation 4 "shuts down" wave constituents that propagate in the "forbidden" direction. This mechanism is demonstrated in the example below.

We have computed the Green's function and its components for a chain with the following parameters. The interparticle distance is $d = \lambda_p/30$. The particles are prolate ellipsoids with axis ratio $1:0.9$ and major semiaxis $a_x = d/3$. The rotation step about $\hat{\mathbf{y}}$ is $\Delta\theta = \pi/3$, creating a chain with period of $N = 3$ particles. The full picture of the Z-plane singularities and their evolution with ω is quite involved, and is discussed in full in Appendix D. Here, we concentrate on the singularities maps within a limited range of frequencies,

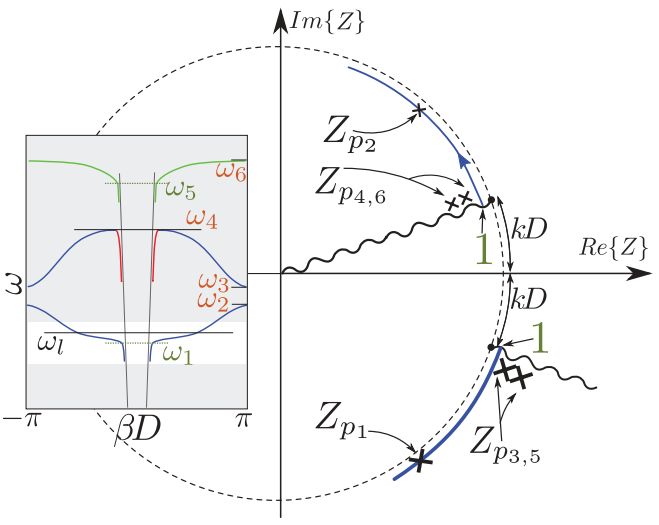

FIG. 9. (Color online) Map of singularities for the chain of longitudinal chirality, without magnetization. Only relevant singularities are shown, corresponding to the frequency range shown by the highlighted strip in the dispersion curves in the inset.

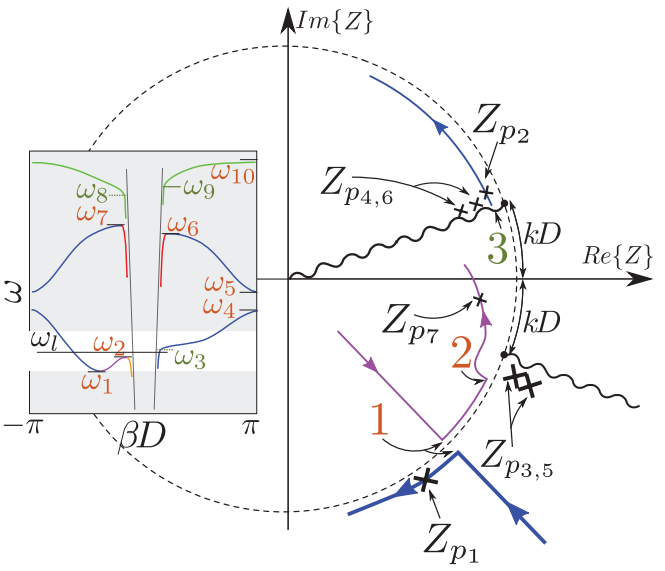

FIG. 10. (Color online) The same as Fig. 9, but for the magnetized chain.

demonstrating the creation of the one-way operation. Typical map of only the relevant singularities that reside on the unit circle, at a given frequency $\omega_l = 0.575625\omega_p$ within that limited range, are shown in Figs. 9 and 10. Being a non-Bravais chain that consists of three particles per period, there are three dispersion curves associated with each chain resonance. These dispersion curves are shown in the insets, and the corresponding frequency range containing ω_l is highlighted. Without magnetization (see Fig. 9), six poles reside on the unit circle in symmetric locations. Two of which ($Z_{p_{1,2}}$) are remote from the branch-point singularity, creating the guided plasmonic modes that propagate to $n > 0$ (Z_{p_2}) and $n < 0$ (Z_{p_1}), see Eq. (14) and the discussion thereafter. Four poles ($Z_{p_{3,4,5,6}}$) reside close to the branch points, formally creating

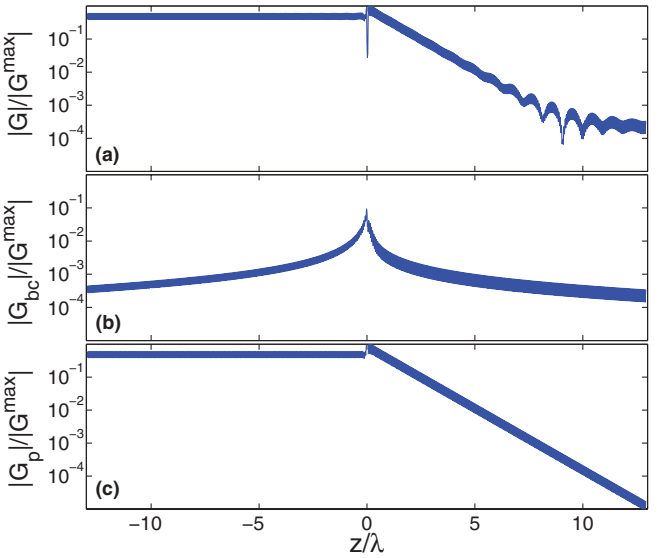

FIG. 11. (Color online) Relative magnitudes of (a) the chain Green's function and its components, (b) CS, and (c) Poles (modes).

two light-line modes that propagate to $n > 0$ ($Z_{p_{4,6}}$) and $n < 0$ ($Z_{p_{3,5}}$). Note, however, that since they are close to the branch points, they are practically not excited (see point 4 above). When magnetization of $\omega_b/\omega_p = 5 \times 10^{-3}$ is applied (see Fig. 10), additional pole appears, and the symmetry of pole locations is lost as predicted in the analysis above. Only a single pole, Z_{p_1}, resides on the unit circle remote from the branch-point singularity, creating a guided plasmonic mode that propagates to $n < 0$. All other poles are either too close to the branch points ($Z_{p_{2-6}}$), or are off the unit circle (Z_{p_7}).

Finally, Fig. 11 shows the Green's function dyad and the contributing components for $\hat{\boldsymbol{x}}$ directed excitation at the first particle of the reference period. The response is shown for each particle in the chain, hence the dense small oscillation (generally $\boldsymbol{p}_n$ is not constant within a period).

V. CONCLUSIONS

A rigorous Greens function theory of one-way particle chains is developed and studied. The theory exposes *all* the wave constituents that may exist and provides an "under the hood" view of the *excitation* properties of these nonreciprocal chains.

In our analysis, we have used the Z transform to obtain a complete spectral representation of the excitation problem. Then, we studied the chains spectra and its analytic properties in the complex spectral (Z) plane, where each and every singularity (e.g., pole, branch point/cut, etc.) represents a distinct wave phenomenon. We explored the breach of symmetry of the complex Z plane singularities, and their manifestations as the symmetry breaking wave mechanisms that underly the one-way guiding effects. It has been shown that this breach of symmetry in particle chains is possible *only* when electromagnetic rotation (caused by magnetization) and geometric rotation (chirality) are *simultaneously* present. Furthermore, it is shown that under this breach of symmetry the CS wave presented by a branch-point singularity practically "shuts down" the modal wave that propagates into the "forbidden" direction, thus playing a pivotal role in establishing the strong nonreciprocal behavior of the chain.

ACKNOWLEDGMENT

This research was supported by the Israel Science Foundation (grant 1503/10).

APPENDIX A: MATHEMATICAL EXPRESSIONS

Here, we summarize some of the mathematical expressions used throughout the main text.

1. Material susceptibility

The magnetized plasma susceptibility tensor $\boldsymbol{\chi}$ is given in Eq. (2), where the entries of $\bar{\boldsymbol{\chi}}$ are given by[22]

$$\bar{\chi}_{xx} = \bar{\omega}^2 + i\sigma\bar{\omega}, \tag{A1a}$$

$$\bar{\chi}_{yy} = \bar{\chi}_{xx} - (1 + i\sigma/\bar{\omega})^{-1}\bar{\omega}_b^2 \sin^2\gamma, \tag{A1b}$$

$$\bar{\chi}_{zz} = \bar{\chi}_{xx} - (1 + i\sigma/\bar{\omega})^{-1}\bar{\omega}_b^2 \cos^2\gamma, \tag{A1c}$$

$$\bar{\chi}_{xy} = -\bar{\chi}_{yx} = i\bar{\omega}\bar{\omega}_b \cos\gamma, \tag{A1d}$$

$$\bar{\chi}_{xz} = -\bar{\chi}_{zx} = -i\bar{\omega}\bar{\omega}_b \sin\gamma, \tag{A1e}$$

$$\bar{\chi}_{yz} = \bar{\chi}_{zy} = -(1 + i\sigma/\bar{\omega})^{-1}\bar{\omega}_b^2 \sin\gamma\cos\gamma. \tag{A1f}$$

2. Computation of $\Delta'(Z)$

By using Eqs. (22)–(24) and the property in Eq. (25), $\Delta'(Z)$ can be expressed explicitly in terms of Li_s in a structure similar to Eqs. (23) and (24),

$$\Delta'(Z) = -C_c'(Z)[\hat{D}_{xx}(Z) + \hat{D}_{yy}(Z)] - C_x'(Z)[\hat{D}_{xy}(Z) - \hat{D}_{yx}(Z)] \tag{A2}$$

with

$$C_{c,x}' = \frac{k^3}{8\pi\epsilon_0}\frac{1}{Z}\sum_{n=1}^{3}\frac{a_n^{c,x}}{(kd)^n}g_{n-1}^{c,x}(Z), \tag{A3}$$

and where the functions $g_m^{c,x}(Z)$ are given by finite sum of polylogarithm functions whose structure is very similar to the functions $f_n^{c,x}(Z)$ of Eq. (24),

$$g_s^c(Z) = -Li_s[e^{i(kd+\Delta\theta)}Z^{-1}] - Li_s[e^{i(kd-\Delta\theta)}Z^{-1}] + Li_s[e^{i(kd+\Delta\theta)}Z] + Li_s[e^{i(kd-\Delta\theta)}Z], \tag{A4a}$$

$$g_s^x(Z) = -Li_s[e^{i(kd+\Delta\theta)}Z^{-1}] + Li_s[e^{i(kd-\Delta\theta)}Z^{-1}] - Li_s[e^{i(kd+\Delta\theta)}Z] + Li_s[e^{i(kd-\Delta\theta)}Z]. \tag{A4b}$$

Since the arguments of the various Li_s terms above are identical to those associated with Eq. (24), the branch points and cuts of $g_m^{c,x}(Z)$ are identical to those of $f_n^{c,x}(Z)$, and are given in Eq. (26) and the discussion thereafter. Note that the leading term in $\lim_{Z\to Z_b}\Delta'(Z)$ is obtained by the multiplication $g_0^{c,x}(Z)f_1^{c,x}(Z)$ for any of the four possible values of the branch point Z_b. Therefore

$$\lim_{Z/Z_b = x\to 1}\Delta'(Z) = C(1-x)^{-1}\ln(1-x), \tag{A5}$$

where C is independent of Z. Here, we used the fact that $Li_0(x) = x/(1-x)$ and $Li_1(x) = -\ln(1-x)$.

APPENDIX B: ANALYTICITY OF h_n ACROSS THE CUT OF $Z^{1/N}$

We prove the identity in Eq. (35). From Eq. (34), it follows that for all integer m,

$$h_n(kd, Ze^{i2\pi m}, q) = \frac{Z^{q/N}}{N}\sum_{r=0}^{N-1}[e^{i2\pi(m-r)/N}]^q \times f_n(kd, Z^{1/N}e^{i2\pi(m-r)/N}). \tag{B1}$$

Note that the summation index r appears only in the unity roots $e^{i2\pi(r-m)/N}$, and the only role of the index m is shifting these roots. Since r roams over $0, \ldots N-1$, the effect of m is limited to changing the order of summation of the same terms. Hence the equality of Eq. (35).

APPENDIX C: PROOF OF Eq. (37b)

From Eqs. (34) and (37a), it follows that

$$h_n(kd,Z^{-1},q) = \frac{Z^{-q/N}}{N}\sum_{r=0}^{N-1} e^{-i2\pi rq/N} f_n(kd,Z^{1/N}e^{i2\pi r/N}). \tag{C1}$$

By using the transformation $r \mapsto N - r'$, we get

$$\begin{aligned} h_n(kd,Z^{-1},q) &= \frac{Z^{-q/N}}{N}\sum_{r'=N}^{1} e^{i2\pi r'q/N} f_n(kd,Z^{1/N}e^{-i2\pi r'/N}) \\ &= h_n(kd,Z,-q), \end{aligned} \tag{C2}$$

where the last equality is due to the fact that the term $r' = N$ can be replaced by a similar expression with $r' = 0$.

APPENDIX D: Z-PLANE DYNAMICS OF THE SECOND CHAIN

A typical map of singularities for a nonmagnetized chain is shown in Fig. 12. The branch points and their corresponding cuts, given in Eq. (36), are denoted by solid circles and wiggly lines, respectively. There are six poles grouped in three pairs that obey the expected symmetry, i.e., $Z_{p_1} = 1/Z_{p_2}$, $Z_{p_3} = 1/Z_{p_4}$, and $Z_{p_5} = 1/Z_{p_6}$. Pole trajectories as a function of ω are shown by solid lines. The specific pole locations marked by $\times$ and branch-point/cut locations correspond to the frequency ω_l marked in the dispersion inset. Since there are several poles with trajectories that coincide with the unit circle C_1, in the figure, we have separated them by shifting the trajectories outside (inside) C_1 for poles with $v_g \lessgtr 0$. Starting at $\omega = 0$ and at low frequencies, $Z_{p_{1,3,5}}$ ($Z_{p_{2,4,6}}$) are located on the unit circle just below (above) the branch point at $Z_b = e^{-ikNd}$ ($Z_b = e^{ikNd}$), thus creating three light-line

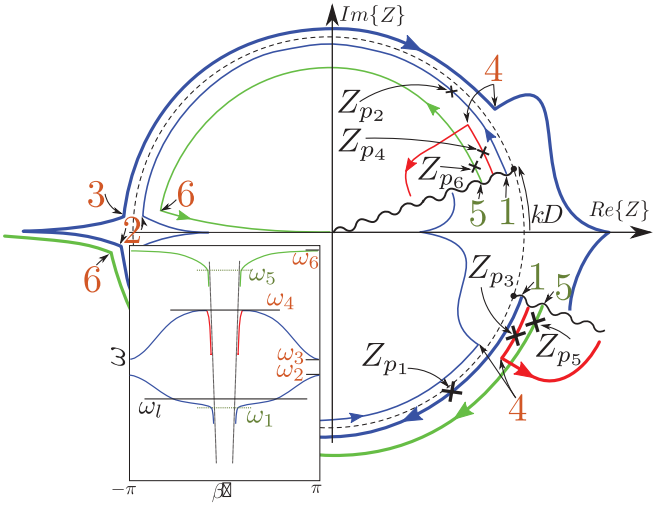

FIG. 12. (Color online) Maps of singularities for the nonmagnetized chain with longitudinal chirality. There are six poles, three of them denoted by thin (thick) lines correspond to modes with positive (negative) group velocity. Note the symmetric locations of the poles, indicating the chain reciprocity. The dispersion for poles that reside on C_1 are shown in the inset, color coded according to the pole trajectories. ω_i corresponds to the ith critical point in the pole trajectory.

modes with dispersion very close to $\beta = \pm\omega/c$. At the critical frequency ω_1, the distance of $Z_{p_{1,2}}$ from their respective branch points increases rapidly thus creating plasmonic guided modes that are detached from the light-line cone, as these poles still evolve along the unit circle and reach point 2 at frequency ω_2 (dispersion curves and pole trajectories in blue). They shift off the unit circle as shown, creating the plasmonic mode upper cutoff. These poles return at frequency ω_3 to the unit circle in point 3 thus creating the lower cutoff of a new plasmonic mode. At point 4 and frequency ω_4, they shift off the unit circle and eventually cross the branch cuts and leave the principal Riemann sheet. We note that up to ω_4, poles $Z_{p_{3,4}}$ evolve near their respective branch points, and then meet $Z_{p_{1,2}}$ at point 4 and as frequency increases, they shift away from the unit circle (red trajectories). Likewise, $Z_{p_{5,6}}$ evolve along the unit circle adjacent to the branch points up to frequency ω_5 at point 5. Beyond that frequency, the distance from their respective branch points increases rapidly thus creating plasmonic guided modes that are detached from the light-line cone, as these poles still evolve along the unit circle and reach point 6 at frequency ω_6 (dispersion curves and pole trajectories in green). Beyond that frequency, they shift away towards the origin (Z_{p_6}) and $-\infty$ (Z_{p_5}).

When magnetization is applied, pole symmetry is lost (but branch point/cut locations are invariant). Maps of singularities for $\omega_b/\omega_p = 5 \times 10^{-3}$ are shown in Fig. 13 together with the corresponding dispersion curves in the inset. Pole locations marked by $\times$ correspond to the frequency $\omega_l = 0.575625\omega_p$ at which the one-way property exists. There is only a single pole, Z_{p_1}, that is located on the unit circle and away from the branch point. All other poles are either off the unit circle thus generating radiation modes that decay exponentially (Z_{p_7}), or adjacent to the branch points ($Z_{p_{2,4,6,3,5}}$). Since the only contributing pole Z_{p_1} evolves along a trajectory that possesses negative group velocity [see Eq. (14) and the discussion thereafter], the chain Green's function excites significantly only towards $n < 0$.

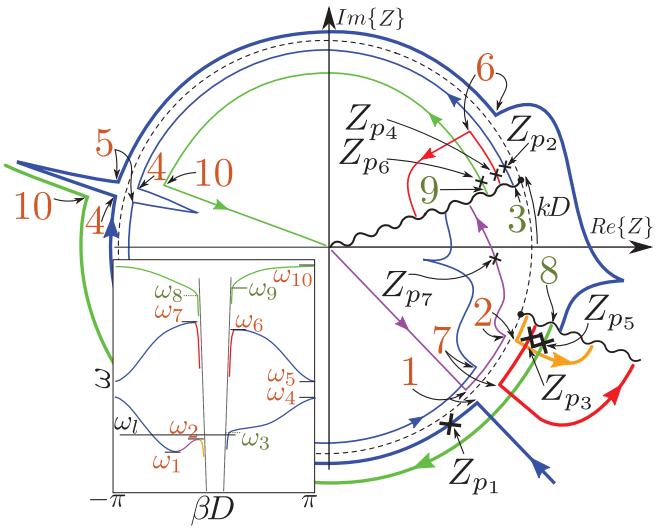

FIG. 13. (Color online) The same as Fig. 12 but for the magnetized chain. There are now seven poles. Symmetry is lost, indicating the chain nonreciprocity.

*Corresponding author: steinber@eng.tau.ac.il

[1]M. Quinten, A. Leitner, J. R. Krenn, and F. R. Aussenegg, Opt. Lett. **23**, 1331 (1998).
[2]S. A. Tretyakov and A. J. Viitanen, Electrical Engineering **82**, 353 (2000).
[3]M. L. Brongersma, J. W. Hartman, and H. A. Atwater, Phys. Rev. B **62**, R16356 (2000).
[4]A. Alu and N. Engheta, Phys. Rev. B **74**, 205436 (2006).
[5]D. V. Orden, Y. Fainman, and V. Lomakin, Opt. Lett. **34**, 422 (2009).
[6]D. V. Orden, Y. Fainman, and V. Lomakin, Opt. Lett. **35**, 2579 (2010).
[7]Y. Hadad and Ben Z. Steinberg, Phys. Rev. Lett. **105**, 233904 (2010).
[8]Y. Mazor and Ben Z. Steinberg, Phys. Rev. B **86**, 045120 (2012).
[9]Y. Hadad and Ben Z. Steinberg, Opt. Express **21**, A77 (2013).
[10]S. S. Walavalkar, A. P. Homyk, M. D. Henry, and A. Scherer, J. Appl. Phys. **107**, 124314 (2010).
[11]Z. Yu, Z. Wang, and S. Fan, Appl. Phys. Lett. **90**, 121133 (2007).
[12]F. D. M. Haldane and S. Raghu, Phys. Rev. Lett. **100**, 013904 (2008).
[13]Z. Wang, Y. D. Chong, J. D. Joannopoulos, and M. Soljacic, Phys. Rev. Lett. **100**, 013905 (2008).
[14]Z. Yu, G. Veronis, Z. Wang, and S. Fan, Phys. Rev. Lett. **100**, 023902 (2008).
[15]Z. Wang, Y. Chong, J. D. Joannopoulos, and M. Soljacic, Nature **461**, 772 (2009).
[16]K. Fang, Z. Yu, and S. Fan, Phys. Rev. B **84**, 075477 (2011).
[17]Y. Hadad and Ben Z. Steinberg, Phys. Rev. B **84**, 125402 (2011).
[18]G. W. Hanson and A. B. Yakovlev, in *Operator Theory for Electromagnetics* (Springer-Verlag, New York, 2002).
[19]L. B. Felsen and N. Markuvitz, in *Radiation and Scattering of Waves* (Prentice Hall, Englewood Cliffs, New Jersey, 1973).
[20]S. A. Maier, P. G. Kik, and H. A. Atwater, Phys. Rev. B **67**, 205402 (2003).
[21]A. H. Sihvola, in *Electromagnetic Mixing Formulas and Applications*, Electromagnetic Waves Series (IEE, London, 1999).
[22]J. D. Jackson, in *Classical Electrodynamics*, 3rd ed. (Wiley, Hoboken, New Jersey, 1999).
[23]S. Campione, S. Steshenko, and F. Capolino, Opt. Express **19**, 18345 (2011).
[24]Leonard Lewin, in *Polylogarithms and Associated Functions* (Elsevier, New York, 1981).